

Chaotic Gas Accretion by Black Holes Embedded in AGN Discs as Cause of Low-spin Signatures in Gravitational Wave Events

Yi-Xian Chen^{1*} and Douglas N. C. Lin^{2,3}

¹*Department of Astrophysical Sciences, Princeton University, USA*

²*Department of Astronomy & Astrophysics, University of California, Santa Cruz, CA 95064, USA*

³*Institute for Advanced Studies, Tsinghua University, Beijing 100084, China*

Accepted XXX. Received YYY; in original form ZZZ

ABSTRACT

Accretion discs around super-massive black holes (SMBH) not only power active galactic nuclei (AGNs), but also host single and binary embedded stellar-mass black holes (EBHs) that grow rapidly from gas accretion. The merger of these EBHs provides a promising mechanism for the excitation of some gravitational wave events observed by LIGO-Virgo, especially those with source masses considerably larger than isolated stellar-mass black hole binaries. In addition to their mass and mass-ratio distribution, their hitherto enigmatic small spin-parameters (χ_{eff}) carry important clues and stringent constraints on their formation channels and evolutionary pathways. Here we show that, between each coalescence, the typical rapid spin of the merged EBHs is suppressed by their subsequent accretion of gas from a turbulent environment, due to its ability to randomize the flow’s spin orientation with respect to that of the EBHs on an eddy-turnover timescale. This theory provides supporting evidence for the prolificacy of EBH mergers and suggests that their mass growth may be dominated by gas accretion rather than their coalescence in AGN discs.

Key words: Accretion Discs – Black Holes – Turbulence – Gravitational Waves

1 INTRODUCTION

Direct observation of the center of our milky way (Ghez et al. 2003; Bartko et al. 2010), as well as abundant tidal disruption event samples (Law-Smith et al. 2017; Mockler & Ramirez-Ruiz 2021) suggest that stellar clusters commonly exist around super-massive black holes (SMBHs) (Kormendy & Ho 2013). In active galactic nuclei (AGNs), the cluster stars may be captured into circularized orbits on the SMBH accretion disc midplane through resonance coupling and gas drag during disc passage (Artymowicz et al. 1993; MacLeod & Lin 2020). Embedded stars may also form *in situ* from gravitational instability (Goodman 2003; Jiang & Goodman 2011; Stone et al. 2017; Chen et al. 2023). Due to the rapid accretion of disc material, they evolve quickly to become massive stars (Cantiello et al. 2021) and then undergo supernova or gravitational collapse, leaving behind not only ejecta that might account for metallicity abundances in AGNs (Hamann & Ferland 1999; Hamann et al. 2002), but also embedded stellar mass black holes (EBHs). Binary stellar-mass black holes (BBHs) may form through dynamical encounters during the global ramp-up of stand-alone EBHs or their local accumulation at migration traps (Bellovary et al. 2016). The hardening and eventual merging of these binaries can be a promising channel to produce gravitational waves (GW) that contribute to LIGO-Virgo events (McKernan et al. 2012, 2014; Yang et al. 2019; Tagawa et al. 2020b; Samsing et al. 2022), especially those with progenitor masses being considerably larger than isolated stellar-mass black hole binaries. Additionally, BBH mergers in an AGN disc may shock-heat the surrounding accretion flow and generate optical/UV flares, an

electromagnetic counterpart that could differentiate them from other merger channels (Graham et al. 2020; Veronesi et al. 2022).

The coalescence of two comparable-mass EBHs generally leads to a merged product with a combined mass M_{\star} and large spin angular momentum J_{\star} (Dones & Tremaine 1993; Hofmann et al. 2016). In a laminar global AGN disc, EBHs with circularized orbits around the SMBH can gain spin angular momentum between merger events through gas accretion from their local circum-stellar discs (CSDs), and quickly become EBHs with high spin aligned with each other (prograde to the disc rotation), even if their initial spins can be negligible (Fuller & Ma 2019). However, the projection of the mass-weighted spin-angular-momentum of individual EBHs in the BBHs’ orbital angular momentum direction (χ_{eff}), inferred from the observed GW events, prefers low values (The LIGO Scientific Collaboration et al. 2021). This distribution suggests low natal EBH spins or random directions between the binary orbital angular momentum and the EBHs’ individual spins (Farr et al. 2017).

While dynamical encounters between BBHs/EBHs and other stars can tilt their orbital planes significantly away from the disc plane, this effect alone cannot reduce the dispersion in χ_{eff} down to typical observational values < 0.1 , and frequent dynamical interactions tend to result in an EBH mass distribution skewed towards higher mass compared with observation (Tagawa et al. 2020b), but see Tagawa et al. (2021) for mitigating this by disruption of soft binaries during binary–binary interactions. It has also been suggested that EBHs or BBHs with non-negligible eccentricity are surrounded by CSDs with retrograde spins (Li et al. 2022; Chen et al. 2022) which introduces misalignment between spin axes of merging EBHs, as possible solutions to this paradox. En route potential paths of BBHs’ migration, ejection and eviction resonances between their precession and

* yc9993@princeton.edu

orbital frequencies can excite eccentricity in BBHs with nearly coplanar and highly inclined orbits whereas spin-orbit resonances can also modify BBHs' obliquity (Gautham Bhaskar et al. 2022).

While fore-mentioned mechanisms rely on misalignment/counter-alignment between EBH populations to produce low- χ_{eff} events, they pose no constraint on the growth of individual EBH spins. Simulations have shown that Blandford-Znajek jet can significantly contribute to spin down of isolated Black Holes (Narayan et al. 2022), although its effect on EBH spin distribution has not been explored in details. On the other hand, sonic-scale magneto-rotational and gravitational instabilities (MRI and GI), commonly occur in AGN accretion discs (Balbus & Hawley 1998; Gammie 2001; Goodman 2003). Both instabilities excite turbulence with locally chaotic eddies. In this paper, we show that EBHs' accretion from strongly turbulent eddies provides an alternative and novel mechanism to robustly reduce the dimensionless spin parameter $a = cJ_{\star}/GM_{\star}^2$ of individual EBHs before they capture or after they merge with their binary companions.

This paper is organized as follows: In §2, we present exemplary numerical simulations that provide insights into how turbulence can affect the spin of CSDs. In §3, we introduce our prescribed models for the spin evolution of individual black holes. Then, in §4, we consider the additional effects of Lense-Thirring torques on spin reorientation and demonstrate that it is not significant in our parameter space of interest. We then apply these methods to study the spin distribution evolution of a population of EBHs in §5 and discuss the implications of our findings in §6.

2 SIMULATION OF CSD FLOW DISRUPTED BY TURBULENCE

2.1 Numerical Setup

To explore the effect of turbulence on the spin re-orientation of embedded CSDs and determine characteristic values of \mathcal{S} , we apply a modified version of the grid-based code FARGO (Masset 2000) with a phenomenological turbulence prescription that follows Laughlin et al. (2004) and Baruteau & Lin (2010).

For our initial conditions, we choose an axisymmetric 2D Keplerian disc model, with the aspect ratio only a function of distance r to the SMBH :

$$h = \frac{c_s}{\Omega r} = h_0 \left(\frac{r}{r_0} \right)^{1/4} \quad (1)$$

where c_s is the sound speed, Ω is the Keplerian frequency and r_0 is the EBH's orbital radius. The code unit is $G = M_{\bullet} = r_0 = 1$, where M_{\bullet} is the central SMBH mass. The EBH's mass ratio is $M_{\star} = qM_{\bullet}$, where $q = 8 \times 10^{-6}$ is our fiducial mass ratio. The EBH companion is placed on circular orbit at $(r, \phi) = (r_0, 0)$. We numerically solve the vertically-integrated hydrodynamic equations in a rotating frame centered on the host star with angular velocity $\Omega(r_0)$, stationary relative to the companion EBH. The gas surface density profile is initialized as

$$\Sigma = \Sigma_0 \left(\frac{r}{r_0} \right)^{-1}, \quad (2)$$

We set $h_0 = 0.03$ and $\Sigma_0 = 1.0$, the latter is simply a normalization constant since we do not calculate gas feedback onto the EBH. Since we focus on the CSDs of EBH, the global radial gradients in h and

Σ do not affect our results. In the companion vicinity $R_B \sim R_H \lesssim H$, where $H = h_0 r_0$ is the global disc's scale height at r_0 , $R_B = GM_{\star}/c_s^2 = 0.009r_0$ is the Bondi radius, and $R_H = r_0(q/3)^{1/3} = 0.014r_0$ is the Hill radius. On a local scale, the resulting flow pattern could correspond to $q \approx 0.3h_0^3$ scaled towards any h_0 (Ormel 2013). This setup represents generally the category of sub-thermal ($R_H < H$) companions. For large SMBH mass $M_{\bullet} \sim 10^8 M_{\odot}$ and $h_0 \gtrsim 0.01$ (Sirko & Goodman 2003), sub-thermal companions should represent the most common kind of EBHs, if $M_{\star} \lesssim 100 M_{\odot}$ consistent with LIGO detections.

To achieve high resolution for studying local physical processes as well as to capture global turbulence qualities, we apply a wedge-like computational domain that extends from $0.6r_0$ to $1.4r_0$ in the radial direction, and $-\pi/8$ to $\pi/8$ in the azimuthal direction, both resolved by 1024 grids with linear spacing. The radial boundary conditions are fixed towards their initial values while the azimuthal boundary condition is periodic.

To prevent gas velocity from diverging infinitely close to the EBH, we consider a smoothed EBH direct potential of the Plummer form, with a grid-scale softening length $\epsilon = 0.1R_B \approx 0.064R_H$ enough to resolve rotation within the CSD but still much larger than the true innermost stable circular orbit (ISCO) of the EBH R_{isco} . Within ϵ (at grid scale), the gravity is softened and gas density inevitably piles up. Realistically, the gas would be compressed onto scales $\sim R_{\text{isco}} \ll \epsilon$. To mitigate the artificial concentration effect on grid scale while leaving gas dynamics at larger scales unchanged by its presence, we introduce a sink term to reduce the surface density gas within ϵ by a factor of f over each numerical (Courant–Friedrichs–Lewy, CFL) timestep τ_{CFL} . The ratio $A \equiv f/\tau_{\text{CFL}}$ factor is controlled to be a constant such that in steady state, a mass removal rate $\int_{|\mathbf{R}| < \epsilon} A \Sigma dS$ is reached where \mathbf{R} is the gas fluid's displacement vector from the companion and dS is unit surface. We set $A = 16\Omega$, but for a sink boundary $< 0.1R_H$ the removal rate has been proven to converge for different A and is usually used as a planetary accretion rate in planet-disc simulations (Tanigawa & Watanabe 2002; D'Angelo et al. 2003). However, since these rates are close to the Bondi rate (Li et al. 2021b) which is much higher than the Eddington rate of EBHs (Li et al. 2022; Tagawa et al. 2022), we expect strong radiation feedback/jets (Jiang et al. 2014, 2019) occurring at scales $\lesssim \epsilon$ but $\gg R_{\text{isco}}$ to significantly recycle out most of that mass flux and leave behind an accretion rate comparable to a few tens to hundreds of Eddington rate that eventually reaches R_{isco} . In our simulation we neglect these effects and assume they do not affect large scale flow structures.

A turbulent potential $\Phi_{\text{turb}} \propto \gamma$ is applied to the disc, corresponding to the superposition of 50 wave-like modes (Laughlin et al. 2004) such that

$$\Phi_{\text{turb}}(r, \varphi, t) = \gamma r^2 \Omega^2 \sum_{k=1}^{50} \Lambda_k(m_k; r, \varphi, t). \quad (3)$$

where γ is the dimensionless characteristic amplitude of turbulence. Each stochastic factor for the k -th mode Λ_k has a wavenumber m_k randomly drawn from a logarithmically uniform distribution between $^1 m = 8$ and the largest wavenumber m_{max} corresponding to wavelength $\sim H^2$. This turbulence driver produces the power spec-

¹ since smaller wavenumbers cannot be accommodated by our wedge-like simulation domain

² This approximates the power spectrum of Graveto-turbulence with a decay below H scale (Booth & Clarke 2019). For MRI one can include up to grid scale turbulence depending on whether small-scale structures are of interest

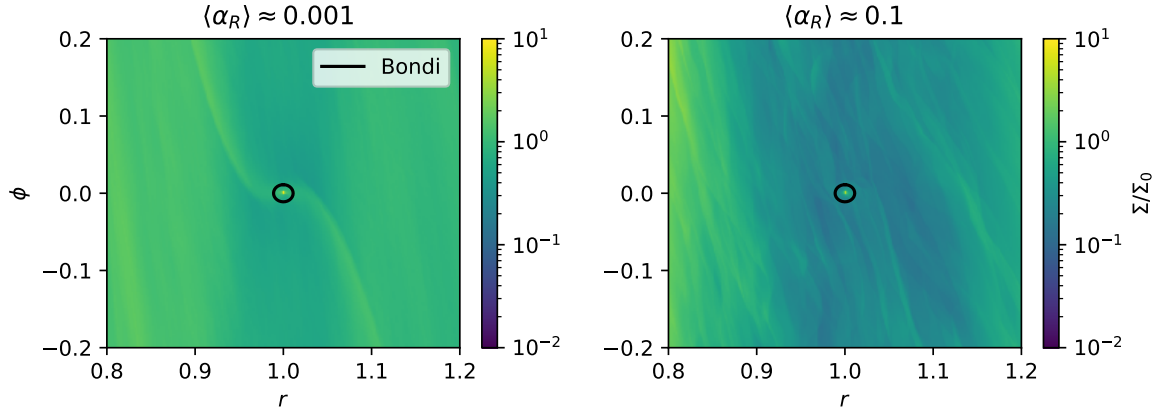


Figure 1. Surface density distribution around the companion when simulation reaches quasi-steady state, averaged over 20 snapshots during one orbital timescale. The normalization density Σ_0 is the initial disc surface density at the companion location. The companion Bondi radius is shown in black lines.

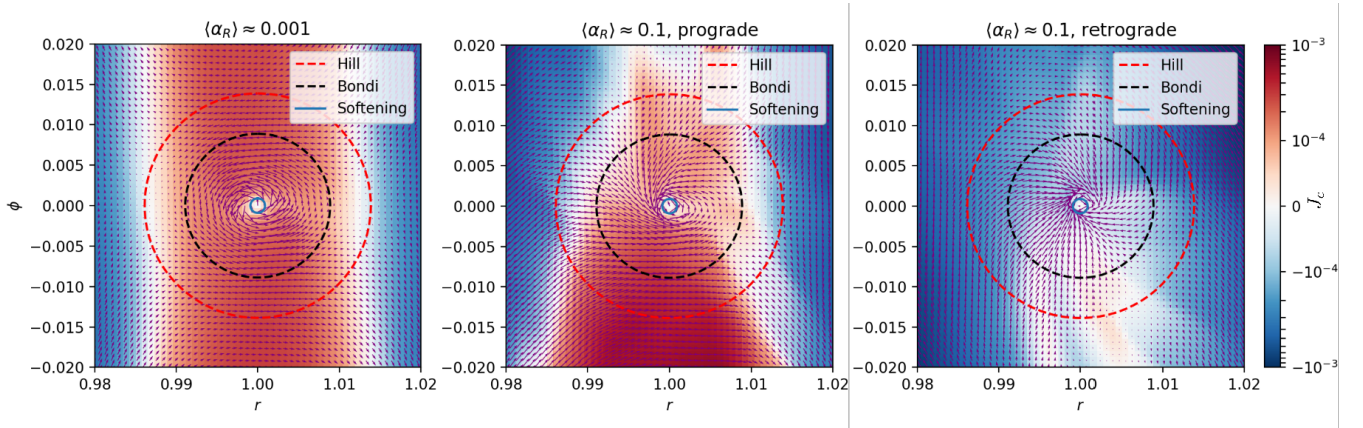


Figure 2. Zoom-in distribution of specific angular momentum with respect to the companion J_c , also averaged over one orbital timescale. Effectively, red means prograde and blue means retrograde. Middle panel and right panel show flow patterns during characteristic prograde and retrograde cycles of CSD flow in the highly turbulent run. Small blue circle, black circle and red circle centered on the companion shows the softening length, Bondi and Hill radius, respectively.

trum of a typical Kolmogorov cascade $m^{-5/3}$ up to m_{\max} , and an effective Reynold stress parameter $\langle \alpha_R \rangle$ around the companion location can be measured from the velocity fluctuations that relates to the turbulence amplitude as $\langle \alpha_R \rangle \approx 35(\gamma/h_0)^2$. (see Baruteau & Lin (2010) for details).

2.2 Results and Implication for EBH Spin-reorientation

We present results from simulations with different γ values, corresponding to $\langle \alpha_R \rangle \approx 0.001$ and $\langle \alpha_R \rangle \approx 0.1$ respectively. From Figure 1, we see that Σ fluctuation in the high turbulence model is much stronger than the low turbulence model. The S-shape density wave, or “wake” induced by companion-disc interaction in a laminar disc (Ogilvie & Lubow 2002) is apparent in the left panel but inconspicuous in the right panel.

We present zoom-in plots of flow patterns in Figure 2. Distribution of specific angular momentum $J_c = |\mathbf{R} \times \mathbf{v}_c|$ is plotted in the

(Laughlin et al. 2004). We confirm that two m_{\max} make little difference since large scale eddies has more influence on the CSD flow.

background of \mathbf{v}_c vectors, representing gas velocity with respect to the companion. In the weak turbulence model (left panel), the steady orbit-averaged flow patterns are very similar to low viscosity or inviscid calculations of planet-disc interaction (D’Angelo et al. 2003; Tanigawa et al. 2012; Ormel 2013). At radii far from the companion the effectively retrograde (blue) Keplerian shear dominates, while closer to the companion weak velocity fluctuation cannot prevent planet tidal potential from establishing a prograde (red) CSD within R_B that connects with horseshoe streamlines at larger azimuth. This means that it’s reasonable to approximate low turbulence with a kinematic viscosity term in laminar fluid equations, as in most planet-disc simulations.

However, in the strong turbulence model corresponding to very large $\alpha_R \gtrsim 0.1$ that gravitational instability in AGN discs may provide (Gammie 2001; Goodman 2003; Deng et al. 2020), this steady-state flow pattern is disrupted and the disc becomes far from laminar. On average during certain individual orbital timescales, the EBH gravity is still able to generate a rotating CSD within the Bondi radius, albeit the typical rotation direction can fluctuate from prograde to retrograde intermittently under influence of turbulence. The middle and right panels of 2 show orbit-averaged result of flow pattern

during a typical prograde CSD episode and a typical retrograde CSD episode.

As an indicator for the general rotation direction of CSD, we calculate the mass-averaged specific angular momentum of gas within the companion Bondi radius (which contains materials instantaneously bound to the companion) excluding the small softened grid-scale region.

$$\langle J_c \rangle_\Sigma = \frac{\int_{\epsilon < |R| < R_B} J_c \Sigma dS}{\int_{\epsilon < |R| < R_B} \Sigma dS} \quad (4)$$

and plot its time evolution in the left panel of Figure 3. In the weak turbulence model, $\langle J_c \rangle_\Sigma$ quickly settles towards a quasi-steady value on the order of $\sim R_B c_s = 0.00027$ in code units, reflecting a steady prograde CSD within the Bondi radius. In the strongly turbulent model, $\langle J_c \rangle_\Sigma$ fluctuates between positive and negative values, giving an overall time average an order-of-magnitude below $R_B c_s$. The right panel of Figure 3 shows the normalized autocorrelation function (ACF) of the time-series $\langle J_c \rangle_\Sigma$,

$$\text{ACF}(\tau) := \frac{\int_{t_{\min} + \tau}^{t_{\max}} \langle J_c \rangle_\Sigma(t - \tau) \langle J_c \rangle_\Sigma(t) dt}{\int_{t_{\min} + \tau}^{t_{\max}} \langle J_c \rangle_\Sigma^2(t) dt} \quad (5)$$

We use $\langle J_c \rangle_\Sigma$ between $t_{\min} = 50$ and $t_{\max} = 100$ orbital timescales to calculate ACF. Measured from the “second-zero-crossing” of ACF function (Oishi et al. 2007; Baruteau & Lin 2010), the ACF timescale is equal to $\Delta t_\star \sim 1 - 2(2\pi/\Omega)$. Statistically, this indicates the typical timescale that rotation of CSD switches direction or the duration of each accretion episode with net angular momentum.

While the CSD flow shows a preferred rotation direction on average over a typical episode (as shown in Figure 2, middle and right panels), the frequency of prograde and retrograde motion cancels out each other. Assuming that either prograde or retrograde rotation can be established down to R_{isco} during each episode, which is beyond the domain of our simulation, it’s reasonable to speculate that the direction of specific angular momentum there, $J_c(R_{\text{isco}})$, will also intermittently flip around due to large-scale flow changes, despite its magnitude remaining around the Keplerian value within each episode (see Eqn 11, which constrain $|J_c(R_{\text{isco}})| \sim \sqrt{GM_\star R_{\text{isco}}}$). To confirm that the episodes cancel out, we define f_J as a proxy to reflect the fractional imbalance between prograde and retrograde flow:

$$f_J = \frac{\int_{\langle J_c \rangle > 0} dt - \int_{\langle J_c \rangle < 0} dt}{\int dt} \quad (6)$$

which is the difference in the duration of prograde episodes v.s. retrograde episodes, normalized by the total duration. While for the laminar case it naturally converges to 100%, we measure $f_J = 0.6\%$ in the turbulent case. The interpretation is that the rotation at small scales will be prograde $\approx 50.3\%$ of the time, while retrograde $\approx 49.7\%$ of the time. If we extrapolate that fraction to the flow rotation down to R_{isco} , it implies a non-stochastic component that would contribute to a net increase of $\approx 0.6\%$ in the value of a in an Eddington timescale. As we will show in the next section, this contribution is smaller than the characteristic dispersion $\sim S^{-0.5}$ contributed by Random Walk (RW). Based on the relatively small imbalance, we infer that in the strong-turbulence parameter space of interest, RW would dominate spin evolution in the long term.

We plot f_J from results of experiments with other values of $\langle \alpha_R \rangle$ in Figure 4, and conclude that for our fiducial set of parameters, $\langle \alpha_R \rangle \gtrsim 0.03$ appears to mark a phase transition from orderly to

more stochastic accretion, and at $\alpha_R = 0.3$ the re-orientation becomes highly random. This transition may be related to fractional diffusion process (a fluctuating factor that gradually decays and a steady-state factor that gradually dominates), the details of which should be explored over larger parameter space by subsequent simulations, possibly with more realistic treatment of turbulence (e.g. with self-gravity and/or radiative cooling).

We also explored another set of simulations with the same mass ratio but $h_0 = 0.01$, which has $R_B > R_H > H$ to represent highly super-thermal companions, common in thin discs $h_0 \sim 0.001$ around low-mass SMBHs (Tagawa et al. 2020a) $M_\bullet \sim 10^6 M_\odot$ or for intermediate mass EBHs (McKernan et al. 2012). In such cases steady-state prograde CSD size is constrained (Martin & Lubow 2011) by R_H , while even high turbulence $\langle \alpha_R \rangle \sim 0.1$ is unable to disrupt the classical prograde flow pattern around EBHs with circular orbits. This result may be expected since the typical turbulence scale H is now smaller than the CSD size, and suggests that transition from orderly to stochastic accretion may have a sensitive mass dependence³. Relaxing the degrees of freedom in 3D simulations might also change the quantitative picture. In this work dedicated to laying out an analytical framework for long-term chaotic spin growth, we simply limit our discussion to sub-thermal companions around high-mass SMBHs and make the following assumptions based on our numerical results:

1) Under influence of strong turbulence, the CSD flow direction of sub-thermal EBHs can become chaotic, with each accretion episode lasting a typical timescale of $\Delta t_\star \sim 2\pi/\Omega$.

2) Our simulation applies 2D geometry, while typical turbulent eddies generated by both gravito-turbulence and MRI become isotropic on scales $< H$ (Beckwith et al. 2011; Booth & Clarke 2019). Taking this effect into consideration, we make an extrapolation to 3D. Instead of switching between prograde and retrograde with respect to the global disc rotation, the dominant eddy that becomes regulated into a CSD by the companion gravity in its vicinity has a fairly isotropic distribution of average inclination θ with respect to the current BH spin, introducing the necessity of including LT effect. However, in Figure 7 we will show that the magnitude of final spins is not sensitive to this extrapolation.

3 LONG-TERM EVOLUTION OF EBH SPIN PARAMETER

The final accretion rate onto the EBHs is likely constrained by the Eddington limit $M_\star = L_E/\eta_\star c^2$, where the EBH luminosity reaches its Eddington luminosity $L = L_E = 1.25 \times 10^{38} M_\star/M_\odot \text{ erg s}^{-1}$, and η_\star is the efficiency factor of EBH accretion. The EBH’s mass-growth timescale is

$$\tau_M \approx \frac{M_\star}{\dot{M}_\star} \simeq \eta_\star \tau_{\text{Sal}} \quad (7)$$

where $\tau_{\text{Sal}} = M_\star c^2/L_E = 4.5 \times 10^8 \text{ yr}$ is the Salpeter timescale. Within an order-of-magnitude, gas in the circumstellar discs (CSDs) is accreted onto the EBHs at R_{isco} with specific angular momentum $|J_c(R_{\text{isco}})| \sim \sqrt{GM_\star R_{\text{isco}}}$, such that in a quiescent environment the spin parameter $|a|$ evolves towards unity on a similar timescale as τ_M .

The accretion efficiency η_\star , which also depends on black hole

³ We note that according to the argument of McKernan et al. (2022), if the spin of high mass EBHs dominating χ_{eff} in extremely unequal mass-ratio mergers tend to be more systematically aligned with the global disc, they can contribute to a large χ_{eff} feature for unequal mass-ratio GW events consistent with observations (Callister et al. 2021).

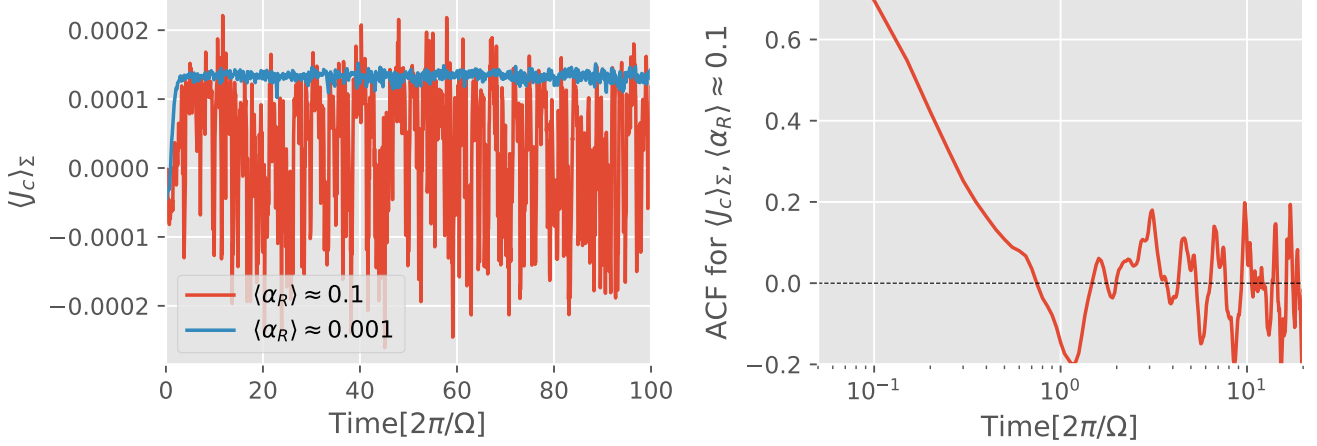


Figure 3. Left: the mass-average specific angular momentum $\langle J_c \rangle_\Sigma$ within the Bondi radius as a function of time. Right: The auto-correlation function of the highly fluctuating $\langle J_c \rangle_\Sigma$ in the highly turbulent simulation, which shows the autocorrelation timescale is close to $2\pi/\Omega$.

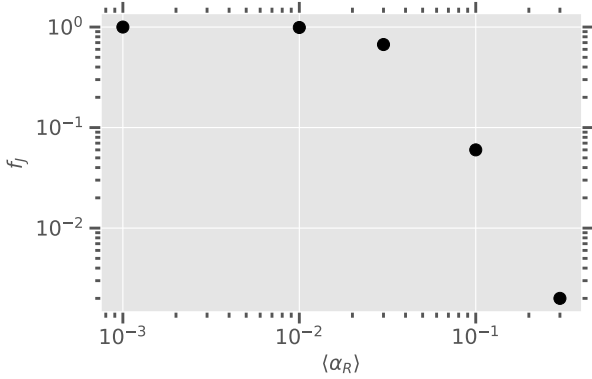


Figure 4. The imbalance (Eqn 6) between total duration of prograde episodes and retrograde episodes, as a function of $\langle \alpha_R \rangle$. This shows for our fiducial set of embedded-companion and disc parameters, the transition from orderly to stochastic CSD spin happens at $\langle \alpha_R \rangle \gtrsim 0.03$

mass and spin, is usually on the order of a few percent for isolated black holes (Jiang et al. 2014, 2019) or even lower due to possible strong outflow/jet for the EBHs in AGN discs (Tagawa et al. 2022), which may provide an important source of heating to the global disc environment. Here we neglect feedback effects as in our simulations, and assume η_\star to be a constant such that τ_M can be a natural unit in our calculations, and $M_\star(t) = M_\star(t=0) \exp(t/\tau_M)$ is a universal mapping of how M_\star evolves with time.

Generally in a turbulent medium, gas accretion occurs in randomly oriented episodes. For SMBH growth over cosmic time, the duration of accretion episodes may be characterised by the timescale that a total “self-gravitating-disc” mass is accreted at the Eddington rate (King & Pringle 2006; King et al. 2008). Alternatively, applied to stellar-mass EBHs in an AGN disc, our simulation shows that the episode timescale is comparable to local dynamical timescale $\Delta t_\star \simeq 2\pi/\Omega \ll \tau_M$, which generally reflects the eddy-turnover or auto-correlation time for MRI and gravito-turbulence (Oishi et al. 2007; Baruteau & Lin 2010; Booth & Clarke 2019). We consider the appropriate cadence limit such that the number of spin-reorientation

episodes during one accretion timescale τ_M is

$$S \equiv \tau_M / \Delta t_\star \simeq \tau_M \Omega / 2\pi = 3 \times 10^4 \frac{\eta_\star}{0.1} \left(\frac{M_\bullet}{10^8 M_\odot} \right)^{1/2} \left(\frac{r_0}{0.3 \text{ pc}} \right)^{-3/2} \quad (8)$$

Since the EBH’s η_\star does not necessarily equal to the SMBH’s accretion efficiency η_\bullet , there are $S\eta_\bullet/\eta_\star$ cycles within the SMBH’s growth timescale or the AGN lifetime. But here we consider $\eta_\bullet \sim \eta_\star$ such that the AGN lifetime is comparable to τ_M of individual EBHs. Given the ratio $\Delta t_\star/\tau_M = S^{-1}$ as the frequency parameter, we numerically model the evolution of EBH spin as a function of time and mass by the following procedure.

1) During one single continuous accretion episode, starting with an initial black hole mass M_0 and initial a_0 , the initial normalized value of $\mathcal{R}_{\text{iseco}} = R_{\text{iseco}}/R_\star$ (R_\star is the Schwarzschild radius) can be calculated from the generic relation between $\mathcal{R}_{\text{iseco}}$ and a (Bardeen 1970; Tagawa et al. 2020b; Reynolds 2021):

$$\mathcal{R}_{\text{iseco}} = 3 + Z_2 - \text{sign}(a) \sqrt{(3 - Z_1)(3 + Z_1 + 2Z_2)} \quad (9)$$

$$Z_1 = 1 + (1 - |a|^2)^{1/3} \left[(1 + |a|)^{1/3} + (1 - |a|)^{1/3} \right] \quad (10)$$

$$Z_2 = \sqrt{3|a|^2 + Z_1^2}$$

The magnitude of $\mathcal{R}_{\text{iseco}}$ ranges from 9 at $a = -1$, to 6 at $a = 0$, then ~ 1 as a approaches unity. In the absence of any discontinuous change in the CSD spin direction and $\mathcal{R}_{\text{iseco}}$, the quantity $\mathcal{R}_{\text{iseco}}^{1/2} M_\star = \mathcal{R}_{\text{iseco}}^{1/2}(M_0, a_0) M_0 := \mathcal{R}_{\text{iseco},0}^{1/2} M_0$ is conserved (Bardeen 1970; King & Pringle 2006), and a evolves as a mapping of M_\star :

$$a(M_\star) = \frac{1}{3} \mathcal{R}_{\text{iseco}}^{1/2} \frac{M_0}{M_\star} \left[4 - \left(3\mathcal{R}_{\text{iseco},0} \left(\frac{M_0}{M_\star} \right)^2 - 2 \right)^{1/2} \right] \quad (11)$$

2) In these classical equations, the sign of a is determined by the directions of black hole angular momentum vector \mathbf{J}_\star and local CSD angular momentum \mathbf{J}_d (specific magnitude of which becomes

relevant in 3D turbulence), such that $a := |a|\text{sign}(\mathbf{J}_\star \cdot \mathbf{J}_d)$ (Tagawa et al. 2020b; Reynolds 2021). But if the direction of \mathbf{J}_d of a population of EBHs changes intermittently due to fluctuating turbulence, this definition of a is unimportant in a collective sense. In our formulation, there is an absolute vertical direction $\hat{\mathbf{z}}$ associated with the global SMBH accretion disc's prograde direction, and only the absolute spin $|a|\text{sign}(\mathbf{J}_\star \cdot \hat{\mathbf{z}})$ may change continuously between switching of EBH accretion cycles, while a alternates between positive and negative values, and $\mathcal{R}_{\text{isco}}$ changes discontinuously (Equation. 9) between values larger and smaller than 6.

The left panel of Figure 5 shows two exemplary individual cases of EBH spin a evolution. By convention, the sign of a is determined relative to the local CSD flow (Bardeen 1970; Tagawa et al. 2020b), or explicitly, $a = |a|\text{sign}(\cos \theta) = |a|\text{sign}(\mathbf{J}_d \cdot \mathbf{J}_\star)$. In a laminar AGN disc, a steady-state CSD flow is either prograde or retrograde with respect to the absolute global disc rotation (Li et al. 2022; Chen et al. 2022), and EBH spin monotonically grow towards this preferred direction. The solid black line shows how an initially counter-aligned $a = -1$ EBH would grow its spin towards the CSD rotation axis, with mass increasing exponentially on the doubling timescale $\tau_M = \tau_{\text{Sal}}\eta_\star$ through Eddington-limited accretion, where τ_{Sal} is the Salpeter timescale and η_\star is the EBH accretion efficiency. In this ideal reference case, we assume initial spin axis is counter-aligned with CSD spin, and in time $\theta = \pi$ would discontinuously jump to $\theta = 0$ as a crosses over to positive, since for $\theta = \pi, 0$ there is no Lense-Thirring (LT) precession torque to change θ continuously. On this ‘‘fundamental track’’, $\mathcal{R}_{\text{isco}}$ shrinks by a factor of 9 as M_\star grows by a factor of 3 from its initial value, reaching an asymptotic limit of $a \simeq 1$ after a timescale of $\tau_M \ln(3)$. EBHs born with spin larger than -1 starts somewhere middle on this same track but the final spins all converge towards 1.

The red line in left panel of Figure 5 shows evolution of a in a fiducial turbulent case with $S = 10^4$. The initial magnitude of the spin is $|a| = 1$, but at the start of every accretion episode with constant duration $\tau_M/S = \tau_{\text{Sal}}\eta_\star/S$, the orientation of CSD spin is randomized with respect to the current EBH spin, and we take account of LT torque in the evolution of θ during every episode. Although a , by definition, oscillates between positive and negative values due to the sporadic shift of CSD spin, through plotting the evolution of $|a|$ in the right panel of Figure 5 in logarithmic scale, we can more clearly see a continuous change in the spin magnitude. We found in the turbulent case, the typical value of $|a|$ first evolves as an exponential decay due to the intrinsic asymmetry between spin-up and spin-down, but after some typical spin-down timescale τ_d comparable to τ_M , random fluctuations around $a = 0$ due to accretion of individual cycles dominate, and characteristic values fluctuate around the random-walk dispersion $a_{RW} \sim S^{-0.5}$. We also tested with $S = 9 \times 10^4$ (right panel, blue line), in which case the random walk factor is smaller, and a longer decay timescale τ_d is needed for the initial spin to decay below this factor. The green dotted line shows analytical prediction $|a| \approx \exp(-2.876t/\tau_M)$, which describes very well the initial spin-down phase. The derivation of this prescription as well as expression $\tau_d \approx \tau_M \ln S/5.752$ are elaborated in Appendix A.

4 EVOLUTION OF SPIN ORIENTATION DUE TO TURBULENCE & LENSE-THIRRING TORQUE

If the effective disc angular momentum that exerts the LT torque is much smaller than the BH angular momentum, the CSD will

generally evolve towards alignment with the EBH if $\theta < \pi/2$ and counteralignment if $\theta > \pi/2$, on a LT timescale of

$$\tau_{LT} = \frac{J_\star}{J_d/\Delta t} \simeq \frac{|a|GM_\star^2/c}{(L_E/\eta c^2)\sqrt{GM_\star R_w}} \simeq \frac{R_\star^{1/2}}{R_w} |a| \tau_M, \quad (12)$$

the warp radius is given by King et al. (2005)

$$\begin{aligned} \frac{R_w}{R_\star} &= 990 \left(\frac{\eta}{0.1}\right)^{1/4} \left(\frac{L}{0.1L_E}\right)^{-1/4} \left(\frac{M_\star}{10^8 M_\odot}\right)^{1/8} \\ &\times \left(\frac{\alpha_1}{0.03}\right)^{1/8} \left(\frac{\alpha_2}{0.03}\right)^{-5/8} |a|^{5/8} \\ &\approx 100 |a|^{5/8} := \mathcal{R}_{w,0} |a|^{5/8} \end{aligned} \quad (13)$$

where α_1, α_2 are the accretion and warp-propagation viscosities. We assume the typical value of $\alpha_1 \sim \alpha_2 \sim 0.03$ ⁴, and choose $\mathcal{R}_{w,0} = 100$ relevant to our EBH parameter $M_\star \sim 10 - 100 M_\odot$. We also limit $R_w/R_\star > 1$. In our case we have defined $J_d = (\eta L_E/c^2)\sqrt{GM_\star R_w \Delta t_\star}$ as the angular momentum that flows past the warp radius (King et al. 2008) during one accretion cycle. Note that $J_d = J_c(R_w)M\Delta t_\star$ is generally much larger than $J_c(R_{\text{isco}})M\Delta t_\star$: the former is the total angular momentum responsible for exerting the LT torque, and the latter is only its small fraction that gets directly fed onto the black hole through R_{isco} .

When $\Delta t_\star/\tau_M$ is very small or S is large, generally $J_d \ll J_\star$ and $\tau_{LT} \gg \Delta t_\star$ for moderate values of $|a|$, which means LT torque cannot strongly influence the EBH inclination during any short accretion cycle, and while θ changes randomly between accretion cycles due to jumps in CSD spin axes, the LT effect cannot accumulate in any preferred direction, so the evolution of a is nearly independent of θ . However, $J_d/J_\star \propto |a|^{-11/16}$ increases with a decreasing $|a|$, and $J_d = J_\star$ when $\tau_{LT} = \Delta t_\star$ or $a_{\text{crit}} \simeq (R_w(a_{\text{crit}})/R_\star)^{1/2}/S$, which gives

$$a_{\text{crit}} \simeq (\mathcal{R}_{w,0}/S^2)^{8/11}. \quad (14)$$

For $|a| \gtrsim a_{\text{crit}}$, any initial $\theta > \pi/2$ is generally directed towards π (counter-alignment) by LT torque, but for $|a| \lesssim a_{\text{crit}}$, even $\theta > \pi/2$ might be directed towards $\theta = 0$ on a timescale of $\tau_{LT} < \Delta t_\star$, which leads to a systematic spin-up of the magnitude of $|a|$ until it fluctuates around the quasi-steady value of $\pm a_{\text{crit}}$ ⁵. Thus concluded King & Pringle (2006) in their qualitative analysis relevant for SMBHs, but they did not consider influence of the random walk. We demonstrated in Figures 6 & 7 that the distribution of $|a|$ is dominated by random walk when $1/\sqrt{S} \gg a_{\text{crit}}$, but will show later that we can reduce to their scenario when $1/\sqrt{S} \lesssim a_{\text{crit}}$ which is probable for SMBH growth, although unlikely in our context.

In our turbulent models for EBH spin evolution, at the start of every turbulent episode, we pick the initial inclination of \mathbf{J}_\star with respect to \mathbf{J}_d from a uniform isotropic distribution, equivalent to picking $\cos(\theta)$ from a uniform distribution from -1 to 1 . If $\cos(\theta)$ has changed sign compared to the previous cycle, a would also change sign and we discontinuously update $\mathcal{R}_{\text{isco}}$ with Equation 9, and then evolve a ,

⁴ applying $\alpha_1 \gtrsim 0.1$ directly from our numerical simulation makes little difference

⁵ The exact long-term alignment criterion is $-2J_{\text{BH}} \cos(\theta) < J_d$ (King et al. 2005), therefore technically $J_{\text{BH}} < J_d/2$ is needed to guarantee systematic spin-up for any random θ , but extra order-unity factors do not qualitatively affect our argument

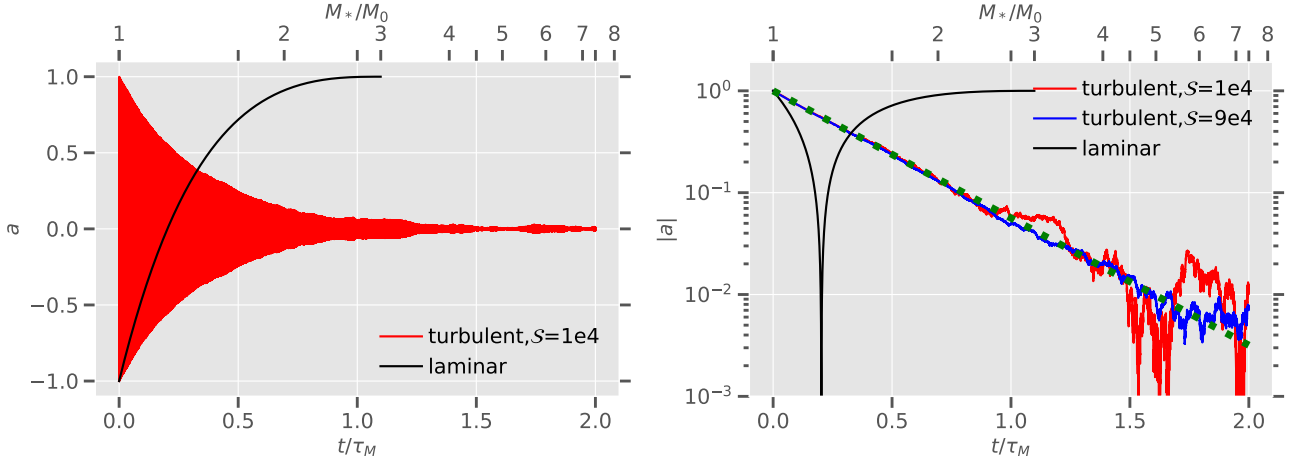


Figure 5. Left panel: Evolution of EBH spin a with sign determined with respect to CSD spin for the laminar case (fixed CSD spin direction, black line), and turbulent case with $S = 10^4$ (red line). In the turbulent case, the CSD spin changes discontinuously every accretion episode so a shifts between positive and negative values with a trend of decaying in magnitude; Right panel: Evolution of $|a|$ in these cases, with an additional $S = 9 \times 10^4$ case shown in blue solid line. The green dotted line shows analytical prediction for the initial spin-down phase, before the spin magnitude becomes comparable to $S^{-0.5}$.

$\mathcal{R}_{\text{isco}}$ continuously again with Equation 11 (replacing $\mathcal{R}_{\text{isco},0}^{1/2} M_0$ with the updated $\mathcal{R}_{\text{isco}}^{1/2} M_*$), until $\cos(\theta)$ changes sign again either due to LT or continuous spin accretion. The short-term continuous local evolution of θ during every accretion timescale of Δt can be calculated by (King et al. 2005)

$$\frac{d}{dt} \cos \theta \approx \frac{1}{\tau_{LT} J_{BH}} \sin^2 \theta (J_d + J_{BH} \cos \theta), \quad (15)$$

where τ_{LT} is used as a normalization for the dissipation term. Note that τ_{LT} is only an estimate of the alignment timescale for moderate values of θ , when $\theta \approx \pi$ the actual timescale becomes much larger than τ_{LT} and approaches infinity at $\theta = \pi$ even if $J_{BH} \ll J_d/2$ since there is no LT precession.

When $\theta < \pi/2$, the time derivative of $\cos(\theta)$ is always larger than 0 and θ decreases towards 0 ($|a|$ consistently spins up). When $\theta > \pi/2$, however, it is worth clarifying that the long-term evolution of θ is not immediately obvious from its local evolution. For example, if $J_{BH} > J_d$ and $\theta \gtrsim \pi/2$ we should have long term counteralignment, but if the initial $\cos(\theta)$ during this cycle is infinitely close to zero or more generally roughly corresponds to a range of $-J_d/J_* \lesssim \cos \theta \lesssim 0$, its derivative is actually positive, which would momentarily align the BH with the disc ($|a|$ spins up momentarily). When that happens, we also update a and $\mathcal{R}_{\text{isco}}$ discontinuously during an accretion cycle before applying Equation 11. This prescription does not contradict the long-term counter-alignment criterion since over a longer timescale $\sim \tau_{LT}$ the EBH would eventually tilt back to become counter-aligned with J_d on timescales comparable to τ_{LT} , see Figure 2 of King et al. (2005). However, practically when $\Delta t_* < \tau_{LT}$, the EBH may not be able to counter-align again before another *new* accretion cycle kicks in and $\cos(\theta)$ is randomized again, so the spin-down is indeed changed to spin-up midway through an accretion cycle even when $J_{BH} > J_d$ in these “lucky” cases. In the “lucky” cases, the EBH spin is momentarily aligned with the disc, may not grow back towards long-term counter-alignment before the next accretion cycle cuts in.

Nevertheless, our result shows that $|a|$ still relaxes towards typical values around $a_{RW} = 1.5S^{-1/2}$, and on average $|a|$ never gets below $a_{\text{crit}} \ll a_{RW}$ for LT torque to have a strong effect and for the eternal-alignment criterion to play a role. This is because the “lucky” cases

roughly corresponds to a range of $-J_d/J_* \lesssim \cos \theta \lesssim 0$, the chance of which happening for isotropic $-1 < \cos \theta < 1$ during every accretion episode is on the order of

$$\left(\frac{J_d}{J_*}\right) \sim \left(\frac{a_{\text{crit}}}{|a|}\right)^{11/16}, \quad (16)$$

which self-consistently is much smaller than order-unity when $|a|$ stabilizes around the the random walk equilibrium $a_{RW} = 1.5S^{-1/2} \gg a_{\text{crit}}$, and the general evolution of $|a|$ still turns out to be random-walk dominated.

By comparing a_{RW} with Equation 14 which shows a_{crit} as a steeper power law of S , we have

$$\frac{a_{\text{crit}}}{a_{RW}} \approx 20 \left(\frac{\mathcal{R}_{w,0}}{10^2}\right)^{8/11} S^{-21/22}. \quad (17)$$

This equation implies that when $\mathcal{R}_{w,0} \gtrsim 100$ and $S \lesssim 20$, a_{crit} may still become larger than a_{RW} . But this range of S is too small to be relevant in the current context, i.e. $\Delta t_* \approx 2\pi/\Omega$.

5 THE POPULATION MODEL, WITH AND WITHOUT LENSE THIRRING EFFECT

In the population models, given the re-orientation parameter S , the spin of 10^3 EBHs are evolved over a timescale of $3\tau_M$, with each initial spin a_0 sampled from a uniform initial distribution from -1 to 1. The initial orientation is also randomly chosen. The initial mass function is irrelevant to the spin evolution in our setup.

In the left panel of Figure 6 we show evolution of average dispersion $\langle a^2 \rangle$ for a population of 10^3 EBHs, starting from a uniform distribution of a between -1 and 1. The root mean square of the spin converges towards an asymptotic value of $a_{RW} \approx 1.5S^{-0.5}$ (red dotted horizontal line), and it does not grow subsequently as it would have in a pure RW. This outcome is due to the competing effect of spin down and RW. With $|a| \approx a_{RW}$, the spin down effect that reduces $|a|$ has stricken an equilibrium with RW diffusion that tends to expand $|a|$. The decay time τ_d is shown as the green dotted

line, which serves as an estimate of the time of transition from initial spin-down-dominated phase to a RW-dominated phase on a population level, since it reflects the slowest possible spin-down timescale of any EBH within this population. The critical spin a_{crit} (black dotted line) below which LT effect becomes important is a sensitive function of \mathcal{S} (see Figure 7). Since the characteristic value of $|a|$ never gets below $a_{RW} \gg a_{crit}$, LT torque does not play a significant role in this evolution process.

In the right panel of Figure 6, we show the histogram for a and $|a|$. Note that due to the slight asymmetry between spin up and spin down with respect to \mathbf{J}_d (spin down is more efficient), the PDF of a has a mean value slightly shifted towards the positive. However by formulation, the \mathbf{J}_d vector distribution is also isotropic, therefore the distribution of spin projection $|a|\text{sign}(\mathbf{J}_d \cdot \mathbf{z})$ with respect to any reference absolute vector \mathbf{z} would essentially be a symmetrically expanded version of the magnitude $|a|$ distribution. We show that the $|a|$ histogram can be approximated very well by Gaussians with dispersion $1.5\mathcal{S}^{-0.5}$ (dashed red line).

To illustrate the relative importance of LT torque, we also run population evolution of EBHs without LT effect, in which we randomly update $\cos(\theta) = 1$ or $\cos(\theta) = -1$ at the beginning of each spin-reorientation episode but do not allow it to evolve, artificially confining the CSD to be either prograde or retrograde with respect to the global disc as in our 2D geometry simulations, just for numerical comparison.

Nevertheless, in the relevant parameter space, the spin evolution is expected to be dominated by random walk (Figure 7, red crosses) and not much different from the 3D model.

As a sanity-check, we demonstrate explicitly that LT torque may still play a large role when a large $\mathcal{R}_{w,0}$ relaxes the viable range of \mathcal{S} for $a_{crit} > a_{RW}$, conforming with previous numerical simulations of SMBH growth (King et al. 2008), first qualitatively suggested King & Pringle (2006). Considering the central SMBH mass $M_\bullet \sim 10^8 M_\odot$, we can choose $\mathcal{R}_{w,0} = 1000$ which is an order of magnitude larger than that in the EBH context. The accretion timescale of King et al. (2008) is defined in terms of the self-gravitational disc mass $\tau_{sg} \sim 0.01\tau_M$, which is similar to $\mathcal{S} \simeq 10^2$. For these parameters, we confirm that $a_{crit} > a_{RW}$. The corresponding a histogram for a population of 10^3 SMBHs after $3\tau_M$ of evolution is shown in Figure 8. In this case, the systematic spin-up by LT torque can prevent any spin-down below $|a| < a_{crit}$, and clear out a central deficit in the distribution function. The spin parameters are strongly peaked around values comparable to a_{crit} , corresponding to equal spin-up and spin-down efficiency (King et al. 2008).

Nevertheless, we emphasize again that this skewed distribution is hard to achieve in our EBH context unless α_2 is very small, especially when $\alpha_2/\alpha_1 = 2 \left(1 + 7\alpha_1^2\right) / \left[\alpha_1^2 \left(4 + \alpha_1^2\right)\right]$ is usually much larger than order unity (Ogilvie 1999). We conclude that in most of the stellar-mass EBH cases RW would dominate, in the sense when $a_{RW} \gg a_{crit}$, the deficit for $|a| < a_{crit}$, although it exists, is negligible in the entire Gaussian distribution.

6 CONCLUSIONS

Results of our hydrodynamical simulations imply that in the limit that the EBH mass is quite small ($\lesssim 100M_\odot$) compared to the SMBH mass ($\gtrsim 10^8 M_\odot$), under influence of strong fluctuating turbulence, the inclination θ between CSD spin vector \mathbf{J}_d and EBH spin vector \mathbf{J}_\star may be frequently randomized, and the growth of EBH's spin occurs through a series of short and independent accretion episodes. The final characteristic magnitude of EBHs' spin is limited by a random

walk (RW) factor on the order of $a_{RW} \sim \mathcal{S}^{-0.5}$, where $\mathcal{S} (\gg 1)$ is the number of CSD spin-reorientation episodes during each Eddington mass doubling timescale. Moreover, the spin axes distribution also becomes isotropic. The characteristic turbulence-coherence (eddy-turnover) timescale is on the order of the local orbital timescale, which gives $\mathcal{S} \sim 10^4$. A final spin distribution with low magnitude and isotropic direction implies a general low- χ_{eff} distribution in subsequent merger events. This outcome is analogous to the low-asymptotic planetary spin due to planetesimal accretion versus the fast spins due to giant impacts (Dones & Tremaine 1993).

We extrapolate the above analysis for stand-alone EBHs to the merging BBHs observed by LIGO-Virgo. If these BBHs form with very close separation and evolve quickly towards coalescence (before the components' spins are significantly modified by three-body encounters and/or multiple-disc interaction), the relative contribution of each member to the merger's χ_{eff} generally cannot exceed the magnitude of a_{RW} of stand-alone EBHs (see Appendix B). In widely separated BBHs, the individuals' spins and the BBHs' orbital angular momentum may still have ample time to evolve and couple as they accret prior to merger. But, if they are surrounded by CSDs with persistent spin orientation, non-negligible quadruple moment in the gravitational potential would induce precession in their orbits. Moreover, either BBHs' modest migration through the global disc or their orbital contraction can lead to eccentricity and inclination excitation through evection and eviction resonances. These effects significantly reduce the magnitude and reorient the direction of BBHs' orbital angular momentum (Gautham Bhaskar et al. 2022). Although these resonances might otherwise be suppressed for those BBHs embedded in CSD with frequent stochastic spin re-orientation ($\mathcal{S} \gg 1$), the cumulative consequence of accretion on the individual components' spins would be analogous to that of the stand-alone EBHs with asymptotic $\sqrt{\langle a^2 \rangle} \sim a_{RW}$, which sets an upper limit to χ_{eff} . An uncertainty in our model is the assumption that the turbulence field in the circum-SMBH is able to rapidly change the circumstellar flow over an eddy-turnover timescale. This assumption can be quantitatively tested with follow-up numerical simulations.

During coalescence of EBHs which might contribute to some of the gravitational wave events detected by LIGO, the EBH mass would increase monotonically with resulting $|a| \sim \mathcal{O}(1)$ (Hofmann et al. 2016). Such growth may account for EBHs' larger masses in comparison with the BHs in Galactic binary systems, but in order to reconcile with the low- χ_{eff} found by LIGO, the coalesced EBHs need to substantially reduce their $|a|$ prior to succeeding coalescence with other EBHs and/or randomize their spin axes. To achieve this, we suggest that EBHs' accretion of GI or MRI-induced turbulent gas in the circum-SMBH discs can lead to both mass increases and $|a|$ decreases.

The highly uncertain EBHs' merger timescale τ_{merge} is determined by many effects including EBHs' migration, mass growth and BBHs' orbital evolution under the influence of circum-BBH discs (Li et al. 2021c,a; Li & Lai 2022) and external secular perturbations (Gautham Bhaskar et al. 2022). The efficiency of these competing mechanisms are beyond the scope of this paper, but we generally conclude that EBHs' mass increase may be primarily due to mergers/gas accretion in the limit $\tau_{merge} \lesssim \tau_M = \tau_{Sal}\eta_\star$ respectively. The latter effect of diminishing $|a|$ is due to the ceaseless re-orientation of the relative angle between the EBHs' spin axis and the angular momentum of the turbulent gas accreted onto them. Considering the spin-down and RW-dominated phase of EBH spin evolution through gas accretion, in the limit $\tau_{merge} \gtrsim \tau_M$, the first phase takes about time $\tau_d = \tau_M \ln \mathcal{S} / 5.752 \sim \tau_M$ to erase any initial spin and the subsequent evolution is dominated by random motion, until the dispersion

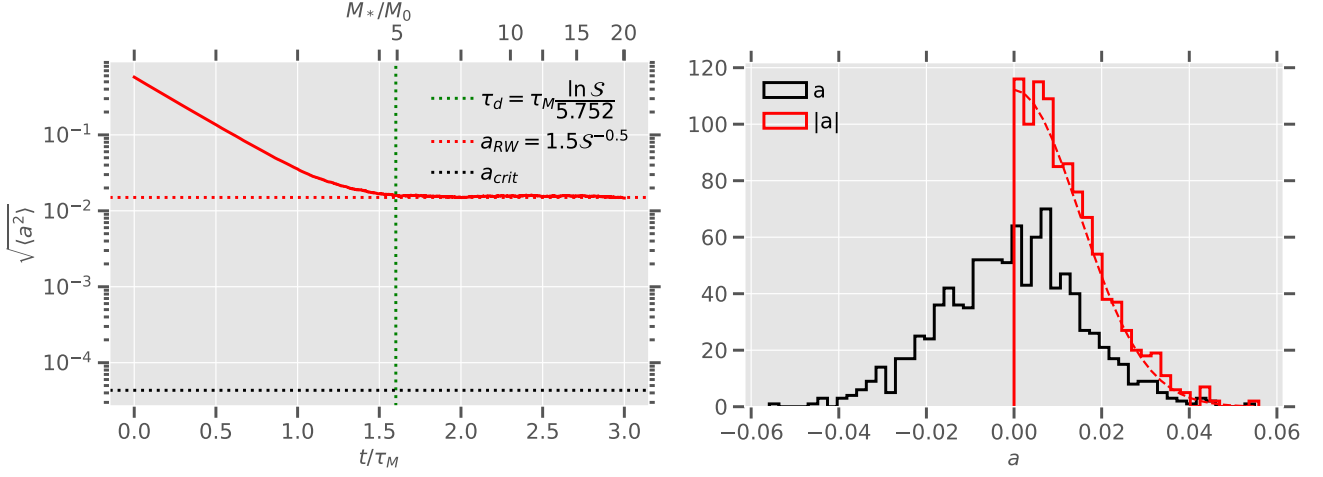


Figure 6. Spin evolution of a population of 10^3 EBHs with $S = 10^4$. Left panel: the root-mean-square of spin parameter, evolving with time, shown in red solid line. The decay time (green dotted line) serves as an accurate estimate of the time where initial $\sqrt{\langle a^2 \rangle} = 1/\sqrt{3}$ (for uniform distribution) decays to the random walk factor a_{RW} (red dotted line), which is much larger than the critical spin (black dotted line) required for systematic spin-up by LT torque; Right panel: The histogram of a and $|a|$ after $3\tau_M$, reaching a semi-steady state. The distribution of $|a|$ can very well be approximated by half a Gaussian with standard deviation a_{RW} .

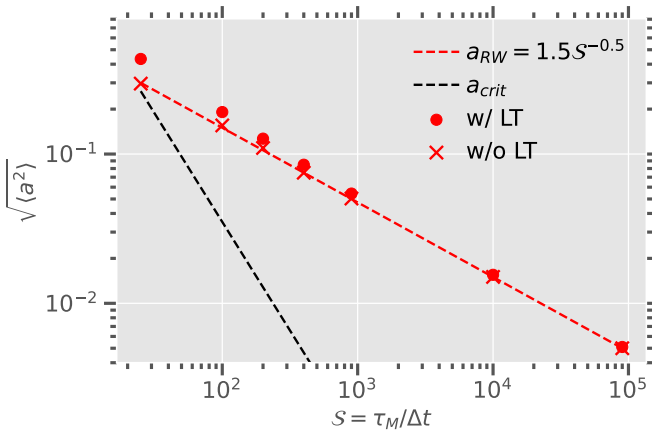


Figure 7. Red dots: The steady-state root mean square spin value of EBH populations after $3\tau_M$ of evolution, varying the spin-reorientation number S . a_{RW} as a function of S is shown in red dashed line and a_{crit} in black dashed line. For large S and $a_{crit} \ll a_{RW}$ we verify that the dispersion converges to a_{RW} , and the $|a|$ histograms are consistently Gaussian. when a_{crit} , a_{RW} becomes comparable, the final dispersion begins to deviate from a_{RW} due to LT effects. Nevertheless, $S \lesssim 100$ is highly unrealistic for the dynamical timescale of disc turbulence and EBH masses.

reaches an asymptotic value $a_{RW} \sim S^{-1/2}$ throughout the AGN duration. The gas-accretion contribution would lead to the small $\chi_{eff} (< 0.1)$ reported by the LIGO detection as well as a significant fraction of EBHs' mass growth. In the limit $\tau_{merge} \lesssim \tau_M$ when merger is very frequent, the first spin-down phase can not be completed and the lowest reachable value for the characteristic spin is $\sqrt{\langle a^2 \rangle} \sim \exp[-2.876\tau_{merge}/\tau_M]$ before merger resets a to $\mathcal{O}(1)$.

We conclude that spin-reorientation of CSDs, fed by rapidly-varying turbulent global disc reconciles efficient gas accretion of EBHs with low spins, and reinforces the scenario that AGN discs are fertile hosting venues for BBH mergers. Furthermore, a low χ_{eff} distribution from observation suggests that EBHs' mass growth is

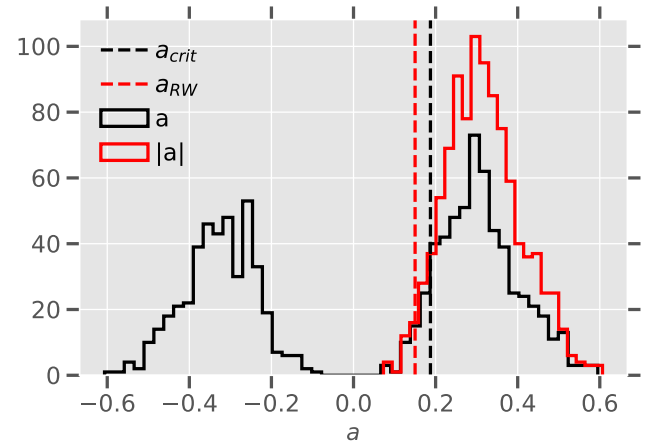


Figure 8. The semi-steady distribution of a and $|a|$ after $3\tau_M$ of evolution for the SMBH context, with $\mathcal{R}_{w,0} = 1000$, $S = 100$. The distribution of $|a|$ can no longer be approximated by Gaussian, but is strongly peaked around values close to a_{crit} (dashed black line), which is already dominating the random walk factor (red dashed line), since systematic spin-up by LT torque can clear out a deficit for any $|a| < a_{crit}$. It can be compared to Figure 4 of King et al. (2008).

dominated by gas accretion rather than their coalescence and the energy dissipated during this process provides intense auxiliary heating sources for the global disc.

Finally, we remark that turbulent eddies can also stifle classical migration torques, limit and randomize radial migration of disc-embedded companions, although this global effect has not been considered in this paper (Laughlin et al. 2004; Baruteau & Lin 2010). The effect of disc turbulence on migration may help to obliterate the current outstanding population-synthesis issue of EBH mass distribution from AGN channel having typical mass that is too large compared with observation, by reducing the efficiency of EBH monotonically migrating into dense clusters around migration traps. While frequent

dynamical interactions in migration traps was traditionally thought necessary to reduce the dispersion in χ_{eff} (Tagawa et al. 2020b), we have shown that turbulent accretion may be more efficient in producing low spin, which relaxes the need for dynamical interactions and in turn does not compulsorily lead to large EBH masses. Since turbulence may mutually constrain EBH spin and mass, this process is a relevant and central effect which should be incorporated in next-generation population models, although the detailed discussion of its specific effect on mass distribution should be the focus of another study. Meanwhile, we note that turbulence is not intrinsically in conflict with other mechanisms concerning dynamical encounters that contribute to specific features in χ_{eff} distribution (McKernan et al. 2022), and they can be combined to give some robust and/or distinguishable prediction in the properties of GW events.

ACKNOWLEDGEMENTS

Y.X.C thanks Clément Baruteau for instructions on the simulation setup. We thank Hui Li, Adam Dempsey, Bhupendra Mishra and Yan-Fei Jiang for helpful discussions. We thank the anonymous referee for valuable suggestions that improved the clarity of the paper.

DATA AVAILABILITY

The data underlying this paper will be shared on reasonable request to the corresponding author.

REFERENCES

- Artymowicz P., Lin D. N. C., Wampler E. J., 1993, *ApJ*, 409, 592
 Balbus S. A., Hawley J. F., 1998, *Reviews of Modern Physics*, 70, 1
 Bardeen J. M., 1970, *Nature*, 226, 64
 Bartko H., et al., 2010, *ApJ*, 708, 834
 Baruteau C., Lin D. N. C., 2010, *ApJ*, 709, 759
 Beckwith K., Armitage P. J., Simon J. B., 2011, *MNRAS*, 416, 361
 Bellovary J. M., Mac Low M.-M., McKernan B., Ford K. E. S., 2016, *ApJ*, 819, L17
 Booth R. A., Clarke C. J., 2019, *MNRAS*, 483, 3718
 Callister T. A., Haster C.-J., Ng K. K. Y., Vitale S., Farr W. M., 2021, *ApJ*, 922, L5
 Cantiello M., Jermyn A. S., Lin D. N. C., 2021, *ApJ*, 910, 94
 Chen Y.-X., Bailey A., Stone J., Zhu Z., 2022, *ApJ*, 939, L23
 Chen Y.-X., Jiang Y.-F., Goodman J., Ostriker E. C., 2023, *arXiv e-prints*, p. [arXiv:2302.10868](https://arxiv.org/abs/2302.10868)
 D’Angelo G., Kley W., Henning T., 2003, *ApJ*, 586, 540
 Deng H., Mayer L., Latter H., 2020, *ApJ*, 891, 154
 Dones L., Tremaine S., 1993, *Icarus*, 103, 67
 Farr W. M., Stevenson S., Miller M. C., Mandel I., Farr B., Vecchio A., 2017, *Nature*, 548, 426
 Fuller J., Ma L., 2019, *ApJ*, 881, L1
 Gammie C. F., 2001, *ApJ*, 553, 174
 Gautham Bhaskar H., Li G., Lin D. N. C., 2022, *arXiv e-prints*, p. [arXiv:2204.07282](https://arxiv.org/abs/2204.07282)
 Ghez A. M., et al., 2003, *ApJ*, 586, L127
 Goodman J., 2003, *MNRAS*, 339, 937
 Graham M. J., et al., 2020, *Phys. Rev. Lett.*, 124, 251102
 Hamann F., Ferland G., 1999, *ARA&A*, 37, 487
 Hamann F., Korista K. T., Ferland G. J., Warner C., Baldwin J., 2002, *ApJ*, 564, 592
 Hofmann F., Barausse E., Rezzolla L., 2016, *ApJ*, 825, L19
 Jiang Y.-F., Goodman J., 2011, *ApJ*, 730, 45
 Jiang Y.-F., Stone J. M., Davis S. W., 2014, *ApJ*, 796, 106
 Jiang Y.-F., Blaes O., Stone J. M., Davis S. W., 2019, *ApJ*, 885, 144

- King A. R., Pringle J. E., 2006, *MNRAS*, 373, L90
 King A. R., Lubow S. H., Ogilvie G. I., Pringle J. E., 2005, *MNRAS*, 363, 49
 King A. R., Pringle J. E., Hofmann J. A., 2008, *MNRAS*, 385, 1621
 Kormendy J., Ho L. C., 2013, *ARA&A*, 51, 511
 Laughlin G., Steinacker A., Adams F. C., 2004, *ApJ*, 608, 489
 Law-Smith J., Ramirez-Ruiz E., Ellison S. L., Foley R. J., 2017, *ApJ*, 850, 22
 Li R., Lai D., 2022, *arXiv e-prints*, p. [arXiv:2202.07633](https://arxiv.org/abs/2202.07633)
 Li Y.-P., Dempsey A. M., Li H., Li S., Li J., 2021a, *arXiv e-prints*, p. [arXiv:2112.11057](https://arxiv.org/abs/2112.11057)
 Li Y.-P., Chen Y.-X., Lin D. N. C., Zhang X., 2021b, *ApJ*, 906, 52
 Li Y.-P., Dempsey A. M., Li S., Li H., Li J., 2021c, *ApJ*, 911, 124
 Li Y.-P., Chen Y.-X., Lin D. N. C., Wang Z., 2022, *ApJ*, 928, L1
 MacLeod M., Lin D. N. C., 2020, *ApJ*, 889, 94
 Martin R. G., Lubow S. H., 2011, *MNRAS*, 413, 1447
 Masset F., 2000, *A&AS*, 141, 165
 McKernan B., Ford K. E. S., Lyra W., Perets H. B., 2012, *MNRAS*, 425, 460
 McKernan B., Ford K. E. S., Kocsis B., Lyra W., Winter L. M., 2014, *MNRAS*, 441, 900
 McKernan B., Ford K. E. S., Callister T., Farr W. M., O’Shaughnessy R., Smith R., Thrane E., Vajpeyi A., 2022, *MNRAS*, 514, 3886
 Mockler B., Ramirez-Ruiz E., 2021, *ApJ*, 906, 101
 Narayan R., Chael A., Chatterjee K., Ricarte A., Curd B., 2022, *MNRAS*, 511, 3795
 Ogilvie G. I., 1999, *MNRAS*, 304, 557
 Ogilvie G. I., Lubow S. H., 2002, *MNRAS*, 330, 950
 Oishi J. S., Mac Low M.-M., Menou K., 2007, *ApJ*, 670, 805
 Ormel C. W., 2013, *MNRAS*, 428, 3526
 Reynolds C. S., 2021, *ARA&A*, 59
 Samsing J., et al., 2022, *Nature*, 603, 237
 Sirko E., Goodman J., 2003, *MNRAS*, 341, 501
 Stone N. C., Metzger B. D., Haiman Z., 2017, *MNRAS*, 464, 946
 Tagawa H., Haiman Z., Kocsis B., 2020a, *ApJ*, 898, 25
 Tagawa H., Haiman Z., Bartos I., Kocsis B., 2020b, *ApJ*, 899, 26
 Tagawa H., Kocsis B., Haiman Z., Bartos I., Omukai K., Samsing J., 2021, *ApJ*, 908, 194
 Tagawa H., Kimura S. S., Haiman Z., Perna R., Tanaka H., Bartos I., 2022, *ApJ*, 927, 41
 Tanigawa T., Watanabe S.-i., 2002, *ApJ*, 580, 506
 Tanigawa T., Ohtsuki K., Machida M. N., 2012, *ApJ*, 747, 47
 The LIGO Scientific Collaboration et al., 2021, *arXiv e-prints*, p. [arXiv:2111.03606](https://arxiv.org/abs/2111.03606)
 Veronesi N., Rossi E. M., van Velzen S., Buscicchio R., 2022, *MNRAS*, 514, 2092
 Yang Y., et al., 2019, *Phys. Rev. Lett.*, 123, 181101

APPENDIX A: ANALYTIC APPROXIMATION OF INITIAL SPIN DECAY

To approximate the mean decay of spin magnitude, we consider an ideal “alternating model” where the CSD spin flips direction every small fraction of the growth timescale $\Delta t = \tau_M/S$ with respect to BH spin, and a switches deterministically between positive and negative values. These flips prevent the magnitude of the EBH spin from increasing monotonically towards $|a| \approx 1$, as in a basic accretion cycle. Instead, we can make a fluctuate around zero without introducing RW diffusion factors. We define

$$\mathcal{R}_{\text{isco},\pm} = 3 + Z_2 \pm \sqrt{(3 - Z_1)(3 + Z_1 + 2Z_2)} \geq 6 \quad (\text{A1})$$

respectively on the spin-down (+) and spin-up (-) branches, so that we do not need to involve $\text{sign}()$ in taking derivatives. Z_1, Z_2 are defined in Equation 10.

Consider two cycles starting from black hole mass M_\star and spin a , each cycle accreting a small amount of material approximately $\Delta M = M_\star \Delta t / \tau_M$, on average a small amount will be chiseled off

$|a|$ because spin down is a little more efficient than spin up. When \mathcal{S} is large, the sign of vector \mathbf{J}_\star is not changed between two small cycles so the switch of \mathbf{J}_d w.r.t. vertical direction is indistinguishable from that w.r.t. \mathbf{J}_\star . As an example, take the first accretion cycle to be spinning down ($a < 0$ regardless of a_{abs}), so we should adopt \mathcal{R}_{isco+} to calculate the reference ISCO radius:

$$\Delta a_1 = M_\star \frac{\Delta t}{\tau_M} \frac{da}{dM_\star} \Big|_{\mathcal{R}_{isco,0}=\mathcal{R}_{isco+}(a)}^{M_0=M_\star}, \quad (\text{A2})$$

After EBH's spin w.r.t CSD grew to be $a + \Delta a_1$, but then the CSD flips so w.r.t CSD the EBH spin parameter becomes $-a - \Delta a_1$, and in this adjacent spin up phase the EBH gains

$$\Delta a_2 = (M_\star + \Delta M) \frac{\Delta t}{\tau_M} \frac{da}{dM_\star} \Big|_{\mathcal{R}_{isco,0}=\mathcal{R}_{isco-}(a+\Delta a_1)}^{M_0=M_\star+\Delta M}. \quad (\text{A3})$$

After two cycles, the CSD spin switches again and a becomes $a + \Delta a_1 - \Delta a_2$. To first order, Δa_1 and Δa_2 scale linearly with Δt since

$$\frac{da}{dM_\star} \Big|_{\mathcal{R}_{isco,0}=\mathcal{R}_{isco,\pm}(a+\Delta a_1)}^{M_0=M_\star+\Delta M} = \frac{da}{dM_\star} \Big|_{\mathcal{R}_{isco,0}=\mathcal{R}_{isco,\pm}(a)}^{M_0=M_\star} + \mathcal{O}(\Delta t). \quad (\text{A4})$$

Neglecting higher order terms, we have from Equation 11 that

$$\frac{da}{dM_\star} \Big|_{\mathcal{R}_{isco,0}=\mathcal{R}_{isco,\pm}(a)}^{M_0=M_\star(t)} = \frac{1}{M_\star} \left(\frac{\mathcal{R}_{isco,\pm}(a)^{3/2}}{(3\mathcal{R}_{isco,\pm}(a) - 2)^{1/2}} - \mathcal{R}_{isco,\pm}(a)^{1/2} [4 - (3\mathcal{R}_{isco,\pm}(a) - 2)^{1/2}] \right) := \frac{\mathcal{F}_\pm(a)}{M_\star}. \quad (\text{A5})$$

The net change in a during a spin-up followed by a spin-down event becomes

$$\Delta a = \Delta a_1 - \Delta a_2 = [\mathcal{F}_+(a) - \mathcal{F}_-(a)] \Delta t / \tau_M. \quad (\text{A6})$$

For $a = 0$, $[\mathcal{F}_+(a) - \mathcal{F}_-(a)] = 0$, so that in the limit $|a| \ll 1$,

$$[\mathcal{F}_+(a) - \mathcal{F}_-(a)] = \frac{d[\mathcal{F}_+(a) - \mathcal{F}_-(a)]}{da} \Big|_{a=0} a + \mathcal{O}(a^2) = -5.752a + \mathcal{O}(a^2). \quad (\text{A7})$$

Note we have approximated the upper limit to be ∞ since the integral from 1 to infinity is also negligible. Since the $\chi < 0$ distribution is completely symmetric, after normalization we have:

which implies that the rate of change for a on average is

$$\frac{\Delta a}{2\Delta t} \approx -2.876a / \tau_M, \quad (\text{A8})$$

When $\Delta t \rightarrow 0$ at $\mathcal{S} = \infty$, the asymptotic limit for a evolution in the alternating case is to alternate between $\pm |a_0| e^{-2.876t/\tau_M}$, while $|a|$ monotonically decreases. Although Equation A7 is valid in the limit of small $|a|$, the exponential function can approximate the entire evolution very well since the initial decay of $|a|$ is quite rapid (See Figure 5, green dotted line). The decay time can be calculated as $\tau_d \approx \tau_M \ln \mathcal{S} / 5.752$, which is the time for $|a_0| = 1$ to reach $|a| = \mathcal{S}^{-0.5}$, while for other values of initial $|a_0|$ the decay time is even shorter. One may also introduce a shortening of $-0.14\tau_M$ in τ_d for reaching the more accurate converged value $a_{RW} = 1.5\mathcal{S}^{-0.5}$ (Figure 6) instead of $\mathcal{S}^{-0.5}$, which is not significant. On a population level, τ_d marks the transition of an initial average spin-down phase towards the steady-state dominated by RW.

APPENDIX B: RELEVANCE TO BBH MERGERS AND χ_{EFF} DISTRIBUTIONS

The detailed influence of an isotropic low-spin distribution on χ_{eff} needs to be understood through population synthesis incorporating mass functions and more detailed physical effects. Nevertheless, we can offer some natural argument asserting that it's difficult for χ_{eff} to reach values much larger than a_{RW} . Once captured into BBHs and after binary inspiral, each individual EBH with mass M_1 and M_2 makes a fractional contribution to χ_{eff} , such that

$$\chi_{\text{eff}} = \frac{M_1}{M_1 + M_2} \chi_1 + \frac{M_2}{M_1 + M_2} \chi_2, \quad \chi_i = |a_i| \cos \psi_i, \quad i = 1, 2 \quad (\text{B1})$$

where ψ_i is angle between EBH spin and binary orbital axis. Avoiding making any specific assumptions about the mass distribution, we understand that in the limit that the evolution towards merger is short, we can draw the magnitude of $|a|$ from the positive part of a Gaussian distribution $f(|a|)$, and $\lambda = \cos \psi$ from a uniform distribution $g(\lambda)$ since the spins have yet to couple with the orbital angular momentum. Neglecting all normalization coefficients, we have the cumulative probability distribution (CDF) for positive $\chi = |a|\lambda$ being

$$\begin{aligned} CDF(0 < \chi < |a|\lambda) &\propto \int_\chi^1 f(|a|) da \int_{\chi/|a|}^1 g(\lambda) d\lambda \\ &\propto \int_\chi^1 f(|a|) \left(1 - \frac{\chi}{|a|}\right) da \end{aligned} \quad (\text{B2})$$

Substituting the exact form of $f(|a|)$, we can derive the probability distribution (PDF) of χ by differentiating the CDF

$$\begin{aligned} PDF(\chi) &\propto -\frac{d}{d\chi} \int_\chi^1 f(|a|) \left(1 - \frac{\chi}{|a|}\right) d|a| = \frac{d}{d\chi} \int_\chi^1 f(|a|) \left(\frac{\chi}{|a|}\right) d|a| \\ &\approx \int_\chi^\infty \exp\left(\frac{-|a|^2}{2a_{RW}^2}\right) \frac{d|a|}{|a|} \propto \mathcal{E}\left(\frac{\chi^2}{2a_{RW}^2}\right), \end{aligned} \quad (\text{B3})$$

$$\mathcal{E}(z) := \int_1^\infty \frac{e^{-xz}}{x} dx = \int_z^\infty \frac{e^{-x}}{x} dx. \quad (\text{B4})$$

$$PDF(\chi) \approx \frac{1}{2\sqrt{2\pi}a_{RW}} \mathcal{E}\left(\frac{\chi^2}{2a_{RW}^2}\right). \quad (\text{B5})$$

This distribution function is very narrow and suggests that χ has $\sim 90.6\%$ probability of being between $\pm a_{RW}$. Since for any general EBH mass function, the mass-weighted average χ_{eff} cannot exceed the value of χ by much, we can constrain the magnitude of χ_{eff} produced from the turbulence channel to be $\lesssim a_{RW}$ for the decoupled spin-orbit angular momentum scenario.

This paper has been typeset from a $\text{\TeX}/\text{\LaTeX}$ file prepared by the author.